Surfactant-assisted electrodeposition of Au–Co/WS2 self-lubricating coating from WS2 suspended cyanide electrolyte

Zhaoxi Chen, Julien Wagner, Viviane Turq, Julien Hillairet, Pierre-Louis Taberna, Raphaël Laloo, Sandrine Nathalie Duluard, Jean-Michel Bernard, Yuntao Song, Qingxi Yang, et al.

Surfactant-assisted electrodeposition of Au–Co/WS_2 self-lubricating coating from WS_2 suspended cyanide electrolyte

Zhaoxi Chen [a, b, *], Julien Wagner [b], Viviane Turq [b], Julien Hillairet [a], Pierre-Louis Taberna [b], Raphael Laloo [b], Sandrine Duluard [b], Jean-Michel Bernard [a], Yuntao Song [c], Qingxi Yang [c], Kun Lu [c], Yong Cheng [c]

[a] CEA, IRFM, F-13108, Saint-Paul-Lez-Durance, France
[b] Institut Carnot CIRIMAT, UMR CNRS-UPS-INP 5085, Université Paul-Sabatier, 118 route de Narbonne, 31062, Toulouse Cedex 9, France
[c] Institute of Plasma Physics, CAS, Hefei, Anhui, 230031, China

A B S T R A C T

In this study, Triton X-100 was used as the WS_2 dispersion agent in the Au–Co cyanide electrolyte to deposit Au–Co/WS_2 composite coatings. Probe sonication was applied to exfoliate the commercial WS_2 powders to produce thinner and smaller WS_2 flakes, which improved the stability of the WS_2 particles in the electrolyte. According to the electrochemical analyses, the effects of adding Triton X-100 and WS_2 particles to the electroplating process were investigated. Through material characterizations, WS_2 par-ticles were proved to be compounded into the Au–Co matrix and showed clearly {002} preferred orientation due to their flake structures. Tribological tests were performed under dry condition in 10^{-3} Pa vacuum against stainless steel 316L balls with diameters of 3 mm and a normal contact force of 2 N. The Au–Co/WS_2 composite coatings that developed showed the minimum coefficient of friction and wear rate of 0.05 and 8×10^{-6} $mm^3/N \cdot m$, which are 5 times and 3 times lower than the Au–Co reference coating, respectively.

Keywords:
Au-Co coating
Electrodeposition
Tungsten disulfide
Triton X-100
Tribology

1. Introduction

As gold (Au) has excellent corrosion resistance, thermal conductivity and electrical conductivity, it is widely used as electrical functional coating on contacts in electronic and telecommunication industries [1,2]. Compared with the Au coating application on the stationary electrical contacts, wear resistance is among the most important performance characteristics of Au coatings on the moving contacts, on which components with intensive movement during normal operation are designed [3]. Electroplating is the preferred industrial technique for Au deposition on metallic substrates and cyanide bath is still commonly used, although it has many safety risks [4]. Adding Ni^{2+} and Co^{2+} as hardening agents into the acidic cyanide electrolytes leads to significant improvements in the coating's mechanical and morphology properties [5–8]. However, in addition to the solid-solution hardening effect and grain size hardening effect, co-depositing of foreign atoms in the Au lattice can also induce lattice distortion, which impairs the electrical conductivity of pure Au coating obviously. Generally, hard Au coatings are hardened by co-depositing of Co with a low content of 0.3–1.6 at.% [9] or Ni less than 2.5 at.% [10].

Implanting nanoparticles in metal matrix coating is another practical approach to enhance the coating's mechanical and chemical properties. Decreasing the particle size is essential not only for promoting homogeneity of composite coatings but also fulfilling the coating thickness requirement in micro-devices, and the particle size that well studied is ranging from 4 nm to 800 nm [11]. One of the biggest challenges is to achieve a uniform and stable micro or nanoparticle suspension in the electrolyte as agglomeration happens easily due to the strong Van der Waals interaction among the nanoparticles. The co-deposition process can be influenced by three main factors: the particle properties, the applied current density and electrode geometry/movement or bath agitation [12]. Investigations of Ni–P [13], Ni [14–17], Co [18], and Cu [19] based composite coatings with carbon nanotubes, graphene solid lubricating nanoparticles were carried out by several authors. In all those cases, the suspension was stabilized by using ionic

* Corresponding author. Building 508, CEA, IRFM, F-13108, Saint-Paul-Lez-Durance, France.
E-mail address: chenzx@ipp.ac.cn (Z. Chen).

https://doi.org/10.1016

surfactants such as sodium dodecyl sulfate and cetyltrimethylammonium bromide. These surfactants have obvious effects on lowering the particles' surface tension to improve their dispersion and/or improving their electrostatic adsorption. The addition of surfactants can also change the zeta potential of the particles in the electrolyte. Even though good wear performance of these composite coatings was achieved, metals used here are prone to be easily oxidized. In contrast, Au based composite coating is less easily oxidized. But in the recent years, there are few literatures reporting the use of Au based composite coating. Carbon-based solid lubricants are broadly used, but they are limited to mild operating conditions. Instead, tungsten disulfide (WS_2) is more compatible in extreme operating environments as it has a high load-carrying capacity, good thermal stability and excellent lubricating performance in high vacuum [20,21]. The attempt of compounding WS_2 in the metal based coating was carried out by some researchers [21–23]. Considering the increasing demand and consumption of Au or Au alloys, the study of compounding WS_2 in Au alloy matrix is interesting, as with WS_2 lubricant compounded, the wear resistance of the Au alloy coating is expected to be improved efficiently even under low contents of foreign alloy elements such as Co and Ni.

It is challenging to achieve a homogeneous – highly required to obtain an even deposition – aqueous WS_2 suspension since WS_2 (0001) surface is made of chemical saturated sulfur atoms making the WS_2 particles hydrophobic [24], leading to large agglomerates in aqueous-based Au plating bath. Even though magnetic stirring is often used for particle dispersion, it has been suspected to be not efficient for WS_2 dispersion [25]. Composite deposition assisted by ultrasonication during electroplating is also reported [26] but gives rise to an apparent heat up of the electrolyte. Another strategy is the use of non-ionic surfactants. Among them, Triton X-100 exhibits high chemical stability in both acid and alkaline electrolytes [27], so that it can be used as the wetting agent in $KAu(CN)_4$ electrolyte [28]. The feasibility of applying Triton X-100 for the Au alloy matrix WS_2 composite coating deposition is interesting to be investigated.

In the present work, the feasibility study of compounding WS_2 nanoparticles in the Au–Co matrix through electrodeposition was carried out. The dispersion stability of WS_2 powder, which was pre-exfoliated by ultrasonication, in the Au–Co cyanide electrolyte with and without Triton X-100 was investigated. The effects of Triton X-100 on the electroplating process were analyzed through electrochemical characterizations. Furthermore, the surface morphology, crystal structure, coating composition, WS_2 distribution in the coating were characterized by means of scanning electron microscopy (SEM), 3D optical profiler, X-ray diffraction (XRD) and energy dispersive X-ray spectroscopy (EDS). Tribological properties of the deposited coatings from different electrolytes with different WS_2 concentrations were studied and compared.

2. Experimental details

2.1. Coating deposition and electrochemical analysis

Recently, CuCrZr becomes an promising base material for the sliding electrical contact development, especially for these work under harsh environment such as in the nuclear fusion experimental devices [29]. CuCrZr plates (10 mm × 8 mm × 2 mm) with 4 μm low-stress electrodeposited Ni interlayers from Ni sulfamate electrolyte as diffusion barriers were used as the substrates in the Au–Co/WS_2 composite electroplating study. Before the deposition, all the substrates were pretreated by a degreasing process with 5 min sonication in acetone and 5 min sonication in ethanol. After the degreasing process, an activating treatment was performed on the Ni surface with 1 min immersion in 20% HCl and 3 min immersion in 25% H_2SO_4 at 25 °C, followed by a quick deionized water rinse and the electroplating was started immediately after that.

The Au–Co electroplating is based on the aqueous cyanide electrolyte from COVENTYA, containing 4 g/L $KAu(CN)_4$, $CoSO_4$, H_3PO_4, and H_2SO_4. The pH of the electrolyte was maintained at 0.6. As Fig. 1 shows, Triton X-100 ($C_{14}H_{22}O(C_2H_4O)n$, n ≈ 10) (Acros Organics) was added into the Au–Co electrolyte reached to a concentration of 8 ml/L with 300 rpm magnetic stirring for 5 min. WS_2 powder (2 μm, ≥ 99%, Sigma-Aldrich) was mechanically exfoliated in deionized water by using a probe sonicator (Vibra Cell 75042, 20 kHz, 500 W, 30% power with 2 s on/2 s off pulses) for 30 min. Then, the exfoliated WS_2 solution was poured to the Au–Co electrolyte containing 8 ml/L Triton X-100 surfactant slowly and agitated with magnetic stirring. By regulating the weight of the WS_2, three Au–Co electrolytes containing 8 ml/L Triton X-100 and different WS_2 concentration (2 g/L, 4 g/L, 8 g/L) were prepared. Besides, three electrolytes (pure Au–Co electrolyte, Au–Co electrolyte containing 8 ml/L Triton X-100, Au–Co electrolyte containing 2 g/L WS_2) were also prepared as references for coating comparison or for WS_2 particle stability study.

In order to evaluate the dispersion state of WS_2 particles in the electrolyte and investigate the mechanism and process of particle aggregation, Turbiscan LAB (Formulaction, France) was applied [30]. During the measurements, specific transparent glass tubes with different electrolytes of 4 cm high were installed in the machine uprightly, and they were scanned by a laser source from the bottom to the top repeatedly. Signal of backscattered (BS) light was detected as a function of time and position along the axis of the tube. The first scanned BS profile was regarded as the reference and after that in each scan, the BS profiles were recorded in delta mode ($\Delta BS = BS_{scan} - BS_{ref}$). From the ΔBS% profile [31], the particles' movement behavior can be recognized. Turbiscan stability index (TSI) can be used to evaluate the dispersion stability, which is defined by the following equation [32]:

$$TSI = \sum_i \frac{\sum_h |scan_i(h) - scan_{i-1}(h)|}{H}$$

where, h and H are the selected height and the total height of the electrolyte sample, respectively. The smaller the *TSI,* the more stable the electrolyte.

In this study, three electrolytes (Table 1) were selected to carry out the WS_2 particle stability study. All the electrolytes were magnetically stirred with a stirrer follower (cylindrical, l = 12 mm, Ø = 3 mm, PTFE) at the tube bottom under the speed of 300 rpm for 5 min, then installed in Turbiscan and measured immediately. The electrolyte samples were scanned each 30 s for 1 h. These tests were carried out at room temperature (25 °C).

The electrodeposition and electrochemical analyses were performed using an electrochemical potentiostat (Gamry Interface 1000, Gamry Instruments, USA). A three-electrode cell was used with a solution volume of 125 mL kept at 45 °C during the plating and electrochemical analysis. The Ni-plated CuCrZr plates (10 mm × 8 mm × 2 mm) were used as the cathode (working electrode) and the counter electrode was a platinum-coated titanium mesh plate (30 mm × 40 mm), with a surface area around 12 cm^2. The plating surface is horizontal and perpendicular to the anode surface with a distance around 25 mm. A platinum wire was used as the quasi-reference electrode, which is suitable for aggressive electrolyte. Linear sweep voltammetry (LSV) measurements were conducted under stirring (120 rpm) in the different plating electrolytes (Table 1). The potential (*vs.* Pt) was scanned between 0 V and −1.5 V at a scan rate of 5 mV/s. The effects of

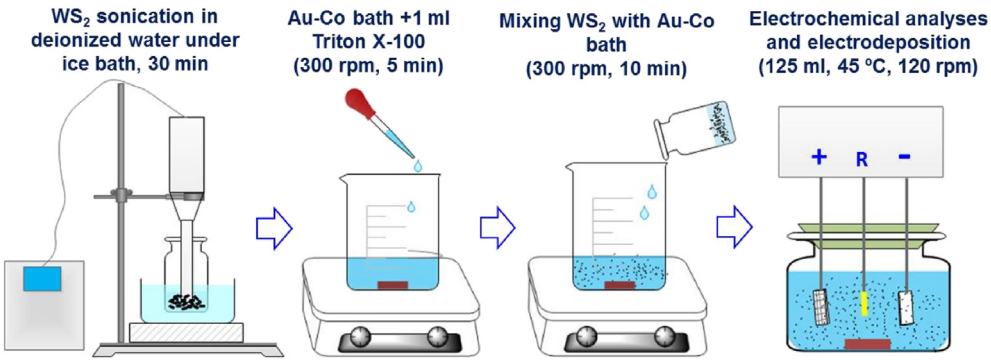

Fig. 1. Sketch of the Au−Co/WS_2 electrolyte preparation process.

Table 1
Electrolytes for the WS_2 particles' stability measurements.

Electrolyte Sample	WS_2 concentration	Triton X-100 concentration	Heating condition
A	2 g/L	–	–
B	2 g/L	8 ml/L	–
C	2 g/L	8 ml/L	45 °C, 40 min

adding Triton X-100 and WS_2 particles in the Au−Co electrolyte on the electrodeposition process were analyzed based on the cathodic polarization curves and the optimum current density that can be used for the composite coating deposition was figured out. Chronopotentiometry study was carried out by using galvanostatic measuring technique with respect to the reference electrode at a current density of 5 A/dm^2 from 0 s to 1000 s.

2.2. Coating characterizations

The morphologies of WS_2 particles, deposited coatings and wear tracks were studied by SEM using the JEOL JSM-5601 electron microscope at an acceleration voltage of 5 kV. The cross-sectional coating samples were prepared by using a cross-polisher (JEOL IB-19510CP, Japan). The compositions of the coatings were analyzed by using an EDS coupled in SEM. The 3D surface measurements were performed on the 3D optical profiler (SENSOFAR, USA), in which the surface roughness of the coating was studied. The crystal structure information including crystal phase and crystallite size of the Au−Co/WS_2 coatings was characterized by using XRD (BRUKER D4 ENDEAVOR, Germany) with Ni filter Cu Kα radiation (λ = 1.542 Å, 40 kV, 40 mA). The X-ray diffraction data were collected from 10° to 100° in 2θ with a 0.0157° step scan. Micro-Raman spectroscopy was applied to investigate the effects of probe sonication to the exfoliation of WS_2 particles. The spectra were recorded at room temperature over a range of 100−2000 cm^{-1}, using a Horiba LabRAM HR800 spectrometer coupled with a 532 nm laser operated at a power of 12 mW. Coatings' tribological performance was evaluated on a ball-on-disc tribometer equipped with high vacuum pumping system against stainless steel 316L ball (Ø = 3 mm). 8000 cycles' rotary sliding tests under dry condition in 10^{-3} Pa vacuum were performed with a linear speed of 6.3 cm/s and a normal contact force of 2 N.

3. Results and discussion

3.1. Morphology of WS_2 particles

Based on the Stokes law, the settling velocity of particles in a Newtonian fluid is proportional to the square of particle diameter [33]. So, reducing the size of the WS_2 particle is beneficial for the dispersion stability of the WS_2 in the electrolyte. For coating aspect, reducing the particles' size especially decreasing their thicknesses by exfoliation can improve their attachment on the substrate surface, which is desirable for increasing WS_2 content in the composite coating.

As Fig. 2 shows, 30 min probe sonication has an obvious effect on the WS_2 particles' morphology, and the averaged WS_2 particle size decreased from 2.8 μm to 1.47 μm. The Raman spectra of the original and the sonicated WS_2 particles are shown in Fig. 2 (d). For the original WS_2 particles, two characteristic active Raman modes were observed at 349 cm^{-1} and 415 cm^{-1}, which correspond to E^1_{2g} and A_{1g}, respectively [34,35]. After probe sonication, the blue-shifting of the E^1_{2g} peak was observed, and this shifting indicates that after probe sonication, the thickness of the WS_2 particles decreased [36]. In addition, compared with the original WS_2 particles, the ratio of intensity between the E^1_{2g} peak and A_{1g} peak increased from 0.75 to 0.82, which is another evidence that shows the exfoliation of WS_2 caused by probe sonication [37,38].

3.2. WS_2 stability in the electrolyte

As Fig. 3 (a) shows, for the electrolyte A without Triton X-100 surfactant, at the bottom (0 mm−0.5 mm) there is a peak with ΔBS % in positive values appears, which indicates the sedimentation of the WS_2 particles. At the top of the tube (38.5 mm−40 mm) there is also a positive peak observed, which indicates that there is a floating layer existing, i.e., creaming occurs. The Au−Co electrolyte shows poor wettability to WS_2 particles and the large surface tension is the reason that induces the creaming of the WS_2 particle. In the middle of the tube, the ΔBS% profiles show large fluctuation, which is dominated by the flocculation and creaming mechanisms. The floating layer can also be observed visually as shown in Fig. 3 (e). In Fig. 3 (b), with 8 ml/L Triton X-100 containing in the electrolyte, the creaming phenomenon is suppressed obviously as the adsorption of Triton X-100 molecules on the WS_2 particle surfaces improves their wettability and decreases the surface tension [39]. Although sedimentation and flocculation are also observed in the electrolyte B, the TSI values of electrolyte B is only half of the electrolyte A (Fig. 4), in which the feasibility of adding Triton X-100

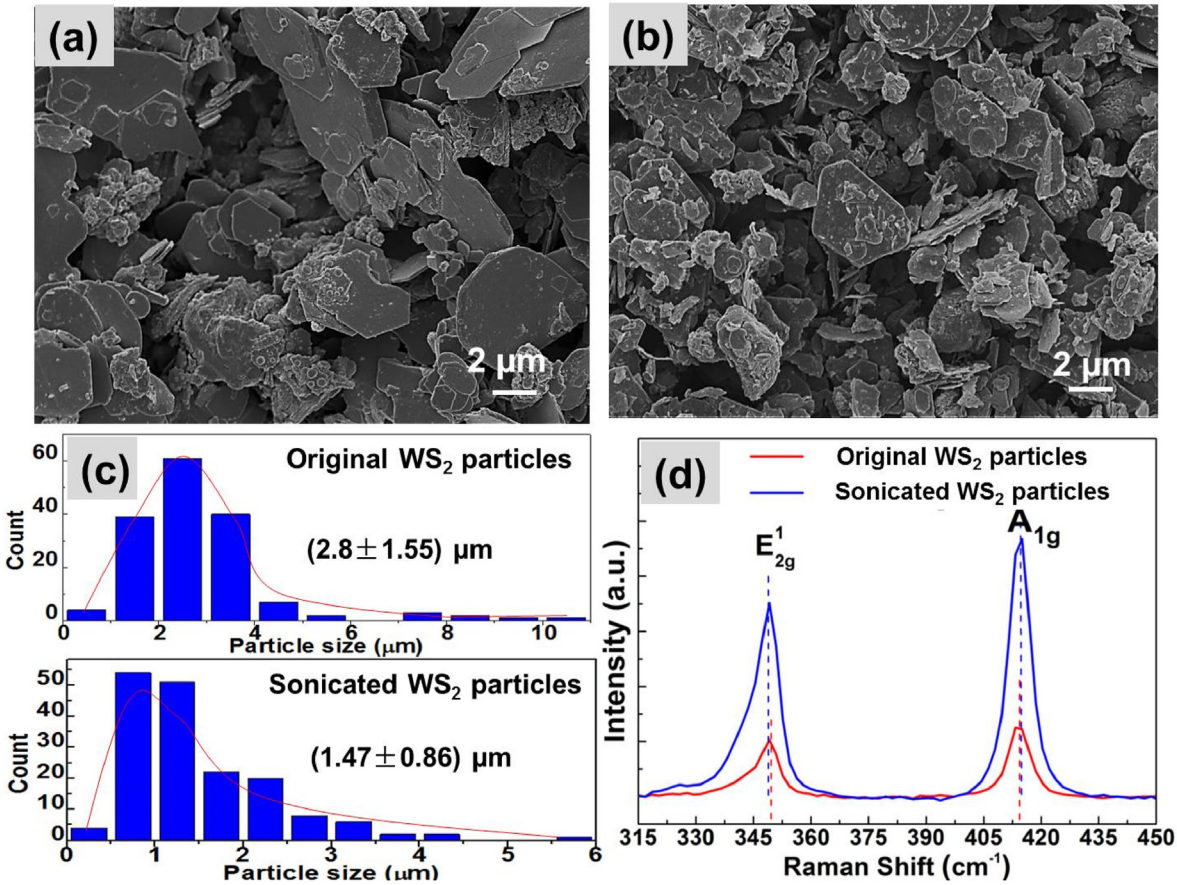

Fig. 2. Effects of probe sonication on the WS_2 particles' morphology: (a). SEM image of the original WS_2 particles, (b). SEM image of the probe sonicated WS_2 particles, (c). Diameter statistics of WS_2 particles before and after probe sonication based on ImageJ software, (d). Raman spectra of WS_2 particles before and after probe sonication.

to improve the Au—Co/WS_2 electrolyte's stability is verified. Especially during 0 min—5 min, the electrolyte B shows high stability as its TSI value is relatively low.

As the optimum deposition temperature of the Au—Co electrolyte is 45 °C, the stability study of WS_2 particles in the 45 °C electrolyte is necessary. Compared with electrolyte B, electrolyte C shows lower stability with higher speed of flocculation and higher tendency of creaming (Fig. 3 (c)). Based on the TSI curve of electrolyte C, something happened after 2 min after the measurement started, as there is a fast transition point observed on the TSI curve.

The property change of the Au—Co electrolyte containing Triton X-100 surfactant maintained at 45 °C for 40 min is illustrated in Fig. 5. Triton X-100 molecule has a hydrophobic tail and a hydrophilic head. When Triton X-100 dissolves into the aqueous electrolyte, the hydrophobic tails of the Triton X-100 molecules orient towards the WS_2 particles' surfaces and the hydrophilic heads associate with water for dissolution [40,41]. The adsorption of Triton X-100 molecules on the WS_2 particle surfaces prevent the WS_2 particles from agglomeration by overcoming the Van der Waals attractions [42]. With magnetic stirring, WS_2 and Triton X-100 molecules present in the electrolyte as micelles uniformly. As a nonionic surfactant, Triton X-100 has a certain temperature (cloud point) in its aqueous solution above which, phase separation occurs [43]. Studies show that the aqueous Triton X-100 solution with a concentration of 1% (v/v) has a cloud point around 65 °C [44]. The large quantities of free ions existing in the Au—Co electrolyte such as $[Au(CN)_4]^-$, SO_4^{2-}, K^+ and PO_4^{3-} can decrease the cloud point of Triton X-100 surfactant. By keeping the Au—Co electrolyte containing 8 ml/L Triton X-100 and 2 g/L WS_2 particles at a temperature of 45 °C for 40 min, the well-dispersed Triton X-100 micelles (with WS_2 particles inside) coagulate and separate as droplets. When the magnetic stirring stopped, sedimentation of Triton X-100 phase which is rich in WS_2 particles appears at the bottom of the cell.

3.3. Linear sweep voltammetry study and galvanostatic electrodepositions

The cathodic reactions during electroplating are expressed as following,

$$[Au(CN)_4]^- + 3e^- \rightarrow Au + 4CN^-$$
$$Co^{2+} + 2e^- \rightarrow Co$$
$$2H^+ + 2e^- \rightarrow H_2\uparrow$$

The cathodic polarization curves measured in the different electrolytes are shown in Fig. 6. As expected, without adding Triton X-100 surfactant and WS_2 particles, the Au—Co electrolyte shows a wide working range of current density from 1 A/dm^2 to 20 A/dm^2. With 8 mL/L Triton X-100 containing in the Au—Co electrolyte, the cathodic onset potential shifts to more negative values and the i-E slope decreases. This indicates that the presence of Triton X-100 in the electrolyte has a significant effect on the Au—Co deposition process, which is attributed to the adsorption of Triton X-100 molecules on the cathode's surface that blocks the active sites and decreases the nucleation rate [45—47].

Compared with the Au—Co electrolyte containing 8 ml/L Triton X-100, adding 0.5 g (4 g/L) WS_2 particles led to a noticeable cathodic overpotential, which should also be assigned to the

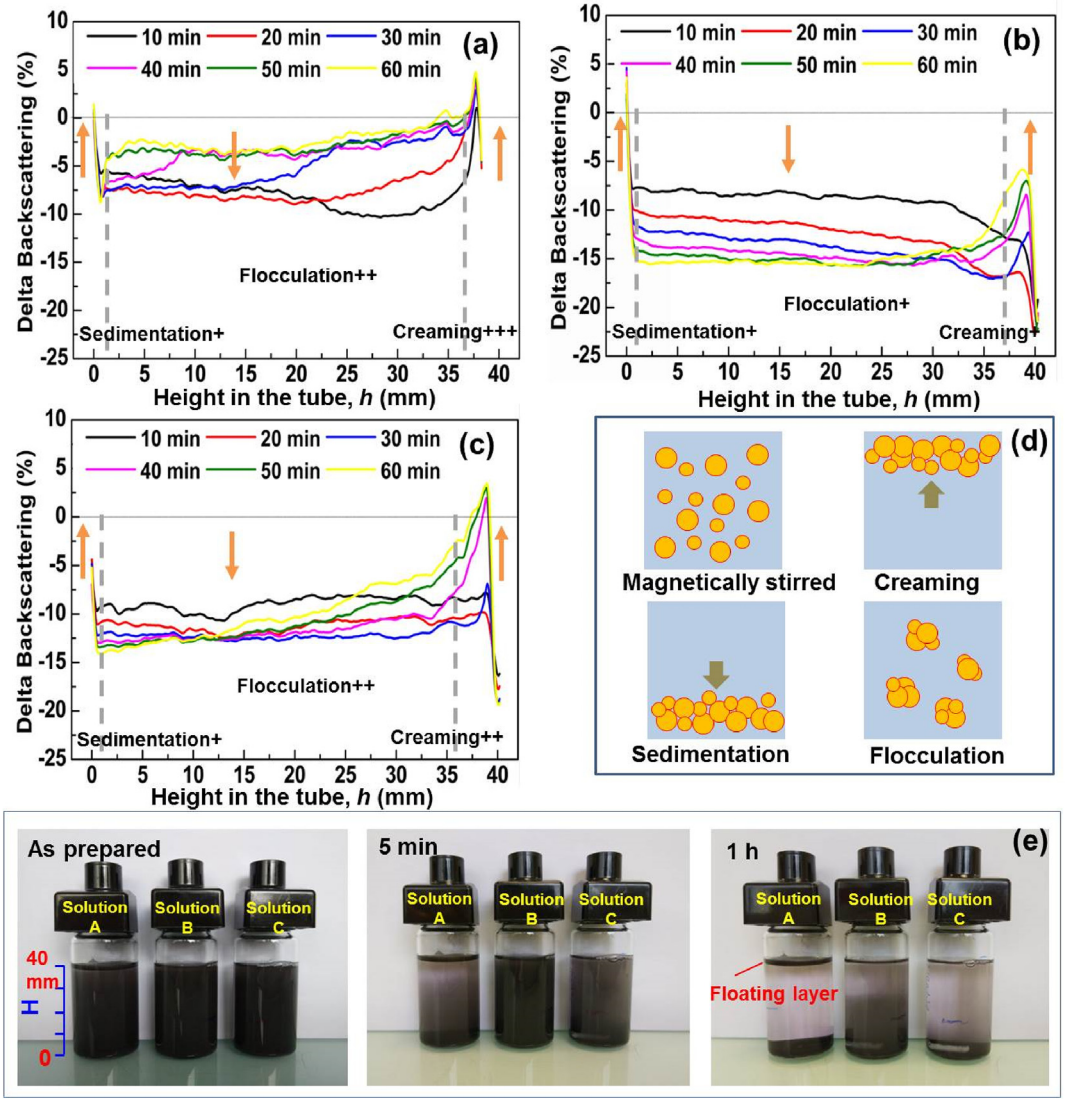

Fig. 3. Results of WS_2 particles' stability measurements: (a,b,c). ΔBS% profiles of the electrolyte A, B and C shown in Table 1 (the quantity of "+" indicates the intensity of the phenomenon) (d). Schematic of WS_2 particles' behavior in the electrolytes, (e). Evolution of the three electrolytes according to the settling time.

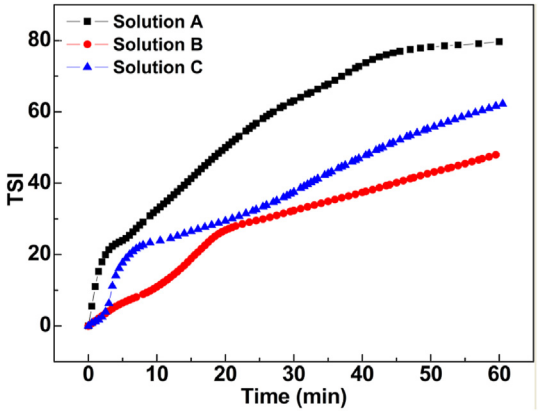

Fig. 4. TSI evolution of different electrolytes over settling time.

adsorption of WS_2 particles on the deposition surface that decreased the active surface area. As observed, significant fluctuations occurred when the current density is higher than 7 A/dm^2, which is linked with the observation of violent hydrogen evolution. In section 3.2, the Au–Co electrolyte containing 8 ml/L Triton X-100 surfactant was observed to have distinct phase separation after being heated at 45 °C for 40 min. After keeping this electrolyte at 45 °C for about 40 min and measuring the polarization curve again, an obvious potential transition to positive side compared with the fresh electrolyte was observed. Especially, when the current density is lower than 7 A/dm^2 the polarization curve of the deteriorated electrolyte is almost the same as the pure Au–Co electrolyte and the violent hydrogen evolution phenomenon postponed in comparison with the fresh Au–Co electrolyte containing 8 ml/L Triton X-100 and 4 g/L WS_2 particles. These evidences indicate that the property of Au–Co electrolyte containing Triton X-100 and WS_2 particles changed with time. According to the polarization curve measurements, 5 A/dm^2 was selected as the current density for the galvanostatic chronopotentiometry study and the Au–Co/WS_2 coating deposition too.

Fig. 7 shows the E-t curves measured at a constant current density of 5 A/dm^2 during electrodeposition in different electrolytes. For the Au–Co electrolyte, the cathodic potential reached to steady-state after a short nucleation stage, and the cathodic

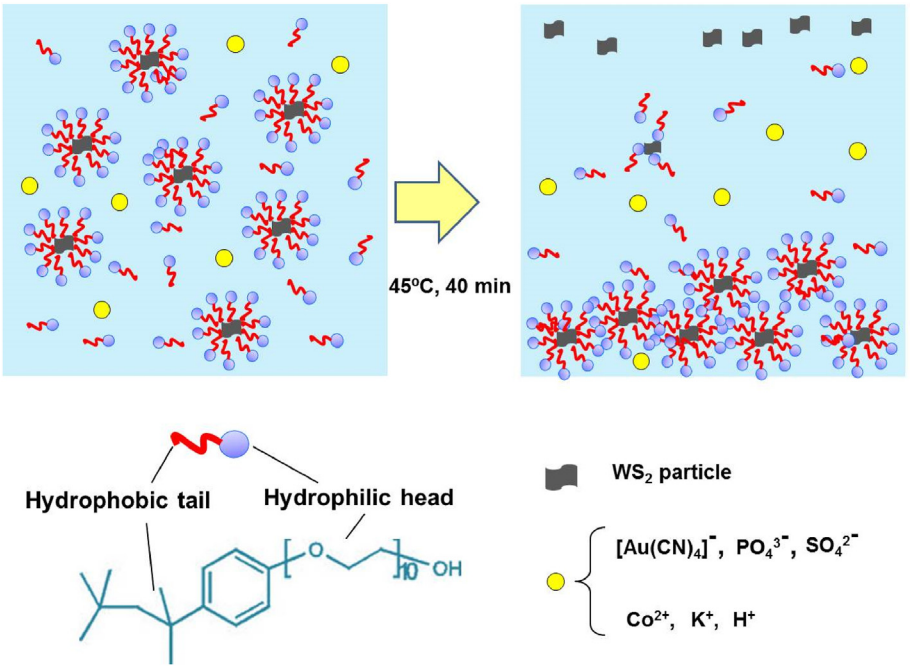

Fig. 5. Schematic illustration of Triton X-100 surfactant assembly on WS_2 particles.

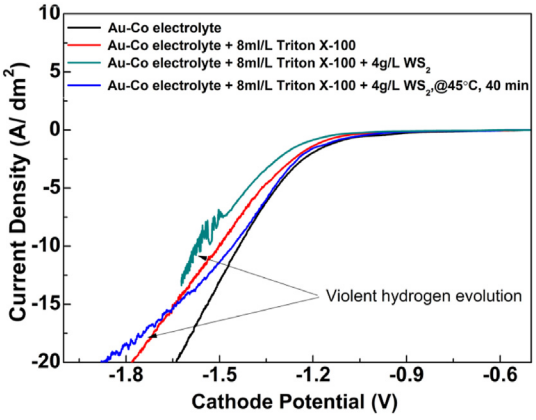

Fig. 6. Cathodic polarization curves measured from different electrolytes.

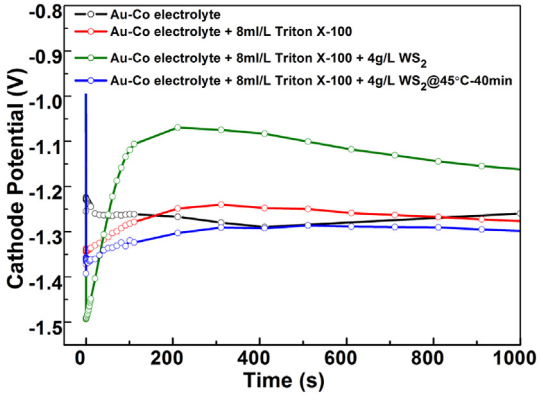

Fig. 7. Potential-time (E-t) curves obtained at J = 5 A/dm^2 from different electrolytes.

potential is about −1.3 V. Cathodic potential decreased to more negative values for the Au–Co electrolyte containing 8 ml/L Triton X-100 surfactant due to the inhibition of Au–Co nucleation. A cathodic potential increase about 0.1 V within 5 min was observed, which is presumably due to the hydrogen evolution as hydrogen evolution needs a lower onset potential (~−0.6 V shown in Fig. 6) than the reduction of $[Au(CN)_4]^-$ (~−1.05 V). For the E-t curve of the Au–Co electrolyte containing 8 ml/L Triton X-100 and 4 g/L WS_2, a similar trend but with more significant cathodic potential variation was observed compared with the Au–Co electrolyte containing only 8 ml/L Triton X-100 surfactant. It's cathodic potential increased from −1.49 V to −1.1 V, under which the $[Au(CN)_4]^-$ reduction was apparently suppressed and the hydrogen evolution turned to the dominant reaction on the cathode.

As referred in the polarization curve measurement section, the degradation of electrolyte containing Triton X-100 and WS_2 particles was also approved with the chronopotentiometric study, which showed that the Au–Co electrolyte containing 8 ml/L Triton X-100 and 4 g/L WS_2 presented a similar E-t behavior as the Au–Co electrolyte after being maintained at 45 °C for 40 min. In order to avoid the influence of the phase separation of the electrolyte on the Au–Co/WS_2 composite coatings' quality, the deposition duration should be less than 40 min.

3.4. Coating rate and compositions

The contents of Co and WS_2 in the Au–Co or Au–Co/WS_2 composite coatings are important for minimizing their wear rate by increasing the hardness and decreasing coefficient of friction (CoF), respectively. As shown in Fig. 8, under the current density of 5 A/dm^2, 0.19 wt% Co in the alloy coating with a coating rate of 0.28 μm/min was achieved by using the Au–Co electrolyte, and the Au–Co coating's hardness is about 250 HV0.01 [48]. With the presence of Triton X-100 (8 ml/L), the coating rate decreased obviously by 50%, which was caused by the low concentration of Co^{2+} and $[Au(CN)_4]^-$ in the electric double layer. When Triton X-100 was added, the cathodic potential shifted to more negative values (Fig. 6) and promoted the reduction of Au (III), which can explain the decrease of Co content in the Au–Co from 0.19 wt% to 0.12 wt%. Due to the Co

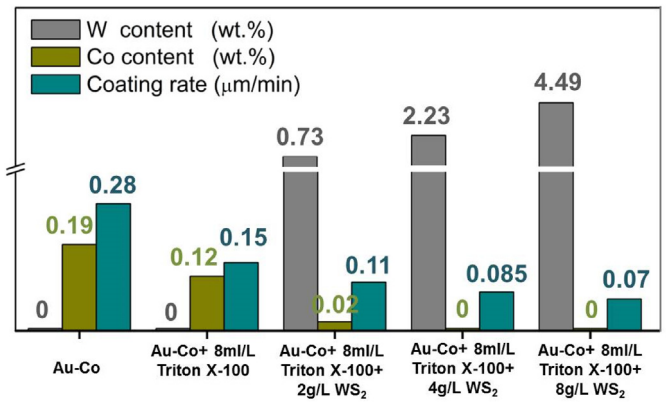

Fig. 8. W, Co contents and coating rates of the deposited coatings from different electrolytes under the current density of 5 A/dm^2.

content decrease, which weakened the solid solution strengthening effect, the Au–Co coating's hardness decreased to 223 HV0.01. For the Au–Co electrolyte containing 8 ml/L Triton X-100 and 2 g/L WS_2 particles, with hydrogen evolution turns up a lower faradic efficiency is obtained, which led to a lower average coating rate (0.11 μm/min). The coating rates decreased with the increase of the WS_2 concentration in the electrolytes. Another obvious effect of mixing WS_2 particles in the electrolytes is the decline of Co contents in the composite coatings, which is also due to the enhancement of cathodic polarization. When the WS_2 concentration is higher than 4 g/L, the Co contents are too low to be measured by EDS technique.

3.5. Coating morphology and topography

As Fig. 9. (a) shows, the electrodeposited Au–Co coating from surfactant-free electrolyte exhibits a surface with relatively large size spherical nodules and a lot of cleavage between them. With Triton X-100 presence in the electrolyte, however, the Au–Co coating surface turned to smother with almost no cleavage observed. Based on the surface roughness measurements, with Triton X-100 added the Au–Co coating surface's arithmetical mean height (Sa) decreased from 0.47 μm to 0.37 μm, and the maximum height (Sz) also decreased slightly (Fig. 10). The reasons that Triton

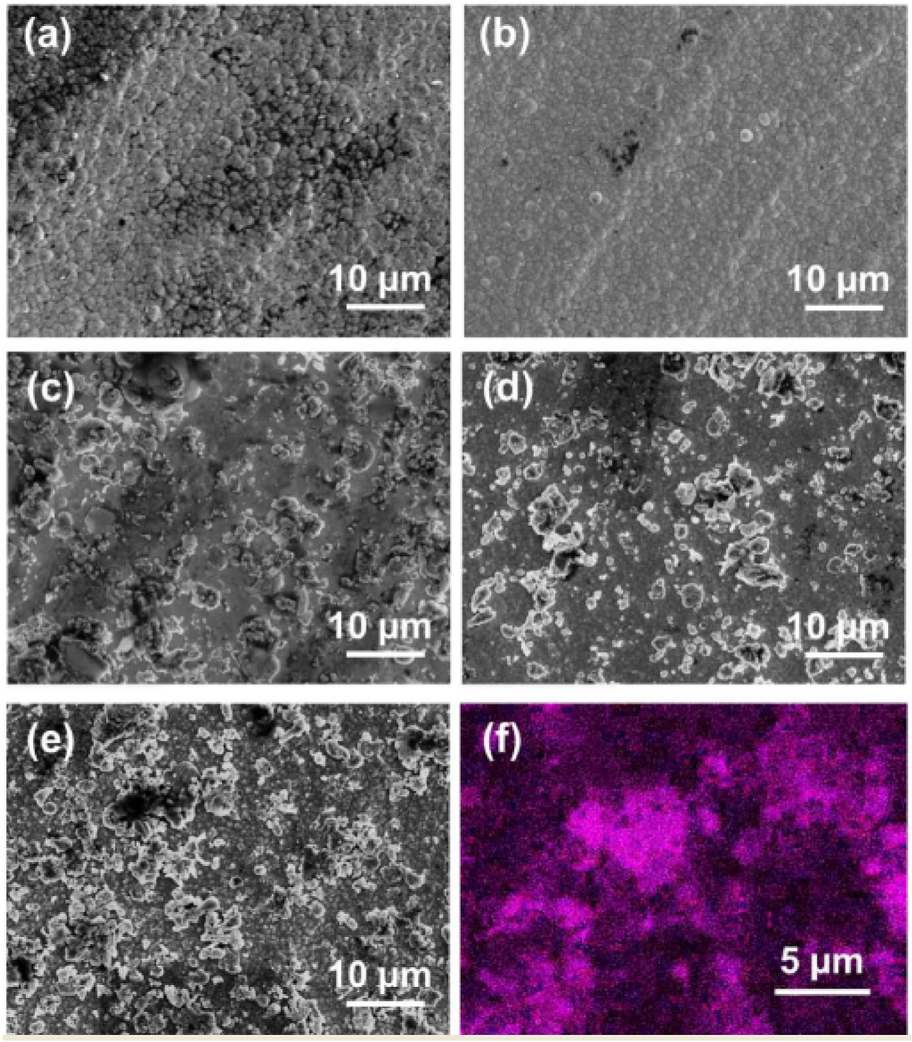

Fig. 9. SEM and EDS images of the electroplated coatings from different electrolytes: (a). Au–Co, (b). Au–Co containing 8 ml/L Triton X-100, (c). Au–Co containing 8 ml/L Triton X-100 and 2 g/L WS_2, (d). Au–Co containing 8 ml/L Triton X-100 and 4 g/L WS_2, (e). Au–Co containing 8 ml/L Triton X-100 and 8 g/L WS_2, (f). EDS mapping of W element (pink color) on the Au–Co/WS_2 coating deposited from the Au–Co electrolyte containing 8 ml/L Triton X-100 and 8 g/L WS_2. (For interpretation of the references to color in this figure legend, the reader is referred to the Web version of this article.)

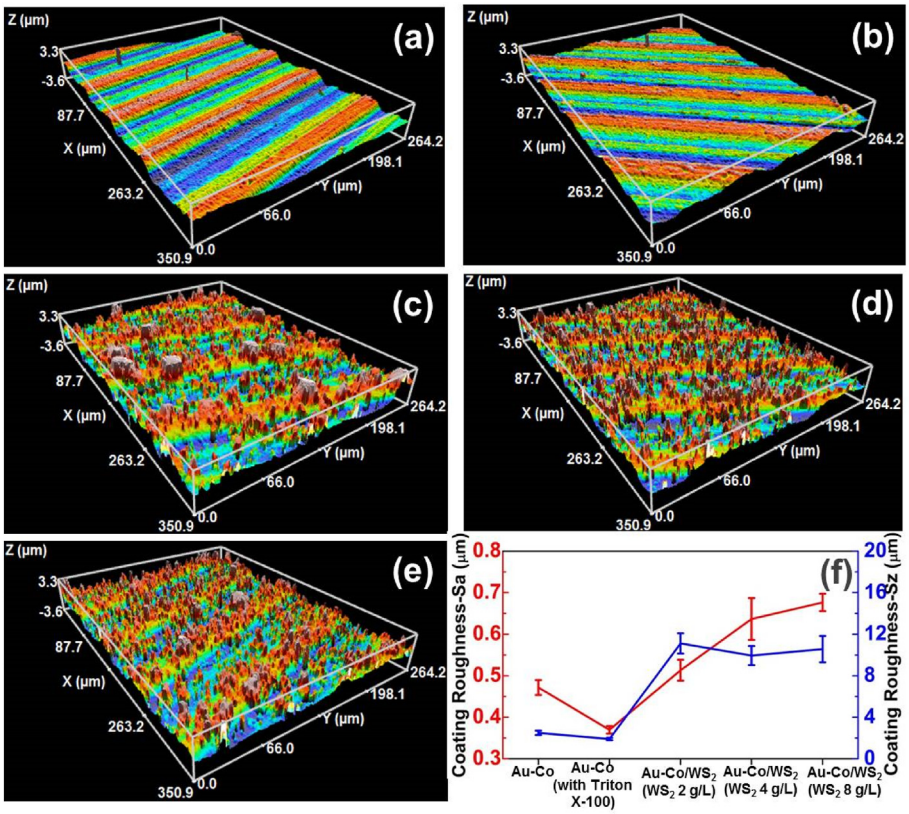

Fig. 10. 3-D surface topography measurements of coatings deposited from different electrolytes: (a). Au–Co, (b). Au–Co containing 8 ml/L Triton X-100, (c). Au–Co containing 8 ml/L Triton X-100 and 2 g/L WS_2, (d). Au–Co containing 8 ml/L Triton X-100 and 4 g/L WS_2, (e). Au–Co containing 8 ml/L Triton X-100 and 8 g/L WS_2, (f). Results summary of Sa and Sz of the deposited coatings.

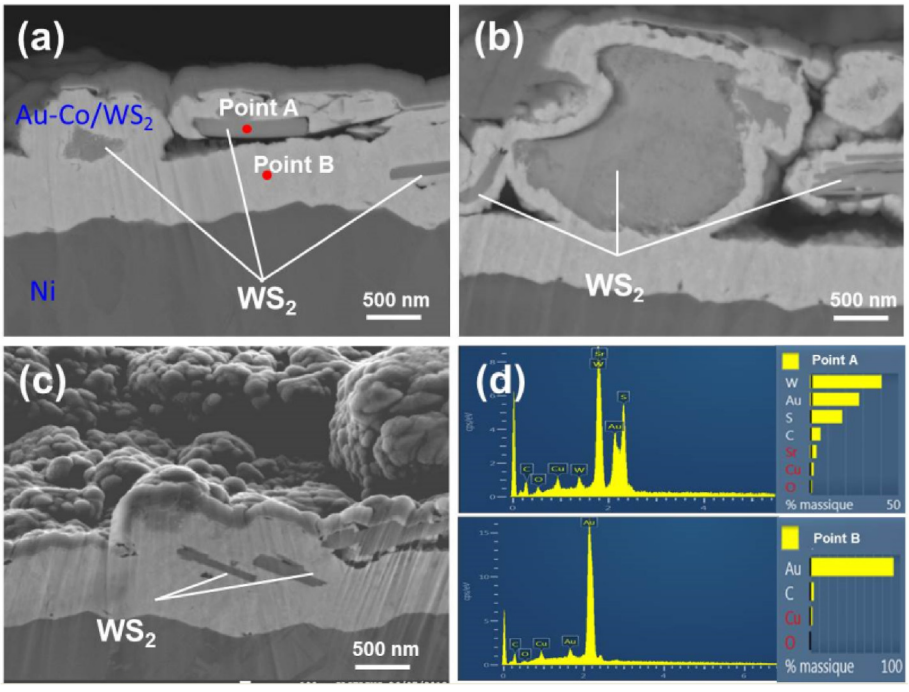

Fig. 11. Cross-sectional SEM and EDS images of the Au–Co/WS_2 coating deposited from the Au–Co electrolyte containing 8 ml/L Triton X-100 and 8 g/L WS_2: (a), (b), (c). SEM images of three different positions on the cross-sectional surface, (d). EDS point analyses at point A and B positions shown in (a).

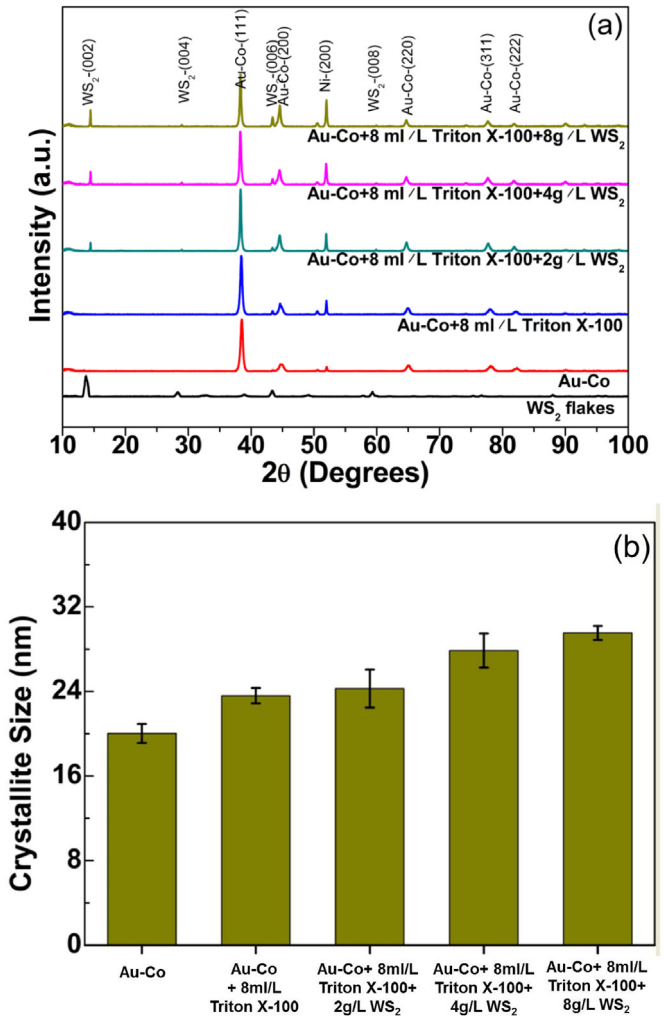

Fig. 12. XRD results of Au–Co and Au–Co/WS_2 coatings: (a). XRD patterns, (b). Crystallite size calculated from Au–Co (111) peaks.

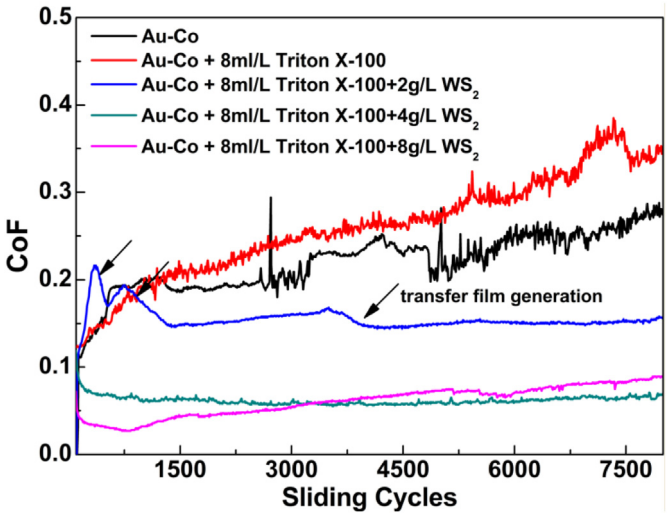

Fig. 13. Coefficients of friction of Au–Co and Au–Co/WS_2 coatings.

X-100 can help to decrease coating surface roughness were due to its functions of filling in gaps and covering a portion of active sites on the substrate, which enhanced uniform nucleation [47,49]. With WS_2 particles added and its concentration increased from 2 g/L to 8 g/L in the electrolyte, the coating surfaces tended to coarse with the appearance of more irregular shape nodules (Fig. 9 (c)–(e)). As shown in Fig. 10, the Sa values of the Au–Co/WS_2 composite coatings with WS_2 particle concentration of 2 g/L, 4 g/L and 8 g/L are 0.51 μm, 0.63 μm and 0.67 μm, respectively. While, the Sz values of the Au–Co/WS_2 coatings are similar, which are around 11 μm. Such protruding structures on the coating surfaces were proved by EDS to be WS_2 clusters embedded into the coatings.

Cross-sectional SEM images of Au–Co/WS_2 composite coating deposited from the Au–Co electrolyte containing 8 ml/L Triton X-100 and 8 g/L WS_2 are shown from Fig. 11 (a) to Fig. 11 (c). The results indicate that the Au–Co/WS_2 composite coating has good bonding interface with Ni interlayer and the Au–Co matrix coating has a dense structure. The WS_2 particles in the composite coating show a clearly preferred orientation, which is parallel to the coating surface, and the thicknesses of the WS_2 particles are around 100 nm–150 nm. As WS_2 particles are semiconductors [50], during deposition, Au–Co nucleation not only occurred on Au–Co surface (initially Ni surface) but also on WS_2 particle surfaces. So, Au–Co growth followed the shape of the WS_2 particles; hence, WS_2 flakes were embedded into the Au–Co matrix compactly.

3.6. Crystal structure

The influence of Triton X-100 and WS_2 particles on the coatings' crystal structure was investigated by using XRD. As Fig. 12 (a) shows, for the WS_2 particles used for the composite coating study, they show crystal planes of (002), (004), (100), (101), (103), (006), (105), (110), (008), (112), (118), etc. All the above planes belong to hexagonal WS_2 [51]. However, in the Au–Co/WS_2 composite coatings, only (002), (004), (006), and (008) diffraction peaks of WS_2 are observed at 2θ of 14.3°, 28.9°, 44° and 59.9°, respectively. Here, only the {002} family of crystal planes were observed, which is another evidence showing that the WS_2 particles show preferential orientation in the coating (with {002} planes parallel to the coating surface). With the increase of WS_2 concentration, the intensities of WS_2 peaks increase accordingly. Crystallite sizes of Au–Co and Au–Co/WS_2 coatings were calculated through the Scherrer equation [52] from Au–Co (111) peaks and the results are shown in Fig. 12 (b). Grain size refinement of the matrix coating was reported with WS_2 particle added in the electrolyte [53]; however, here we found the crystallite size of the Au–Co matrix increased with the adding of WS_2 particles and the presence of Triton X-100. The reason for the crystallite size increase could be probably due to the inhibition of Triton X-100 molecules, which decreased the Au–Co nucleation. The Co content decrease, which is discussed in section 3.4, could be another reason that caused Au–Co crystallite increase.

3.7. Tribological performance

As shown in Fig. 13, for the Au–Co coating obtained from Au–Co electrolyte, the CoF started from 0.15 and increased slowly to 0.3 during the 8000 cycles sliding. With 8 ml/L Triton X-100 added, the Au–Co coating obtained showed worse tribological performance and its maximum CoF reached to 0.4. Based on the coating compositional study and crystallite size study, with the presence of Triton X-100 in the electrolyte, the Co content in the Au–Co alloy coating was suppressed and the coating crystallite size increased. All these factors impaired the hardness of the Au–Co coating and therefore, induced a higher CoF. Au–Co/WS_2 composite coatings showed very different CoFs compared with Au–Co coating. For the

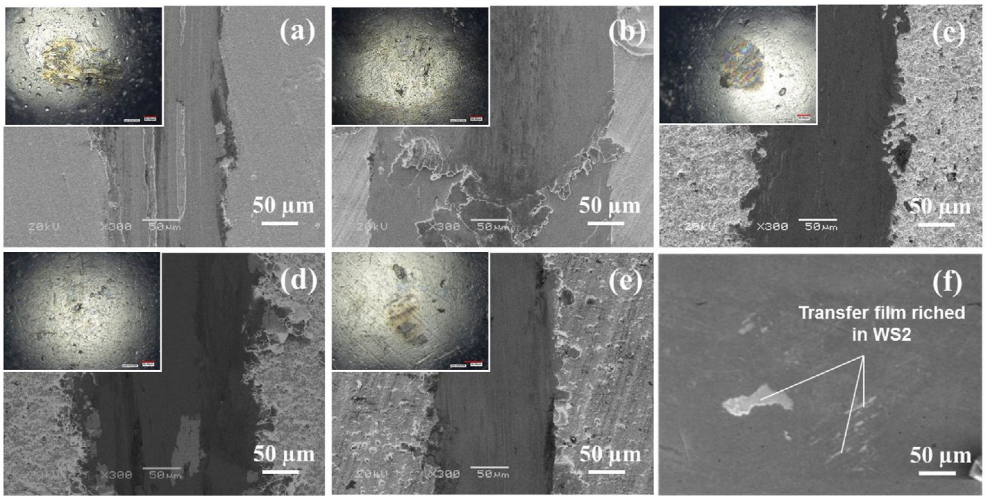

Fig. 14. Worn surface morphologies of different coatings and their counterpart balls: (a). Au–Co, (b). Au–Co containing 8 ml/L Triton X-100, (c). Au–Co containing 8 ml/L Triton X-100 and 2 g/L WS_2, (d). Au–Co containing 8 ml/L Triton X-100 and 4 g/L WS_2, (e). Au–Co containing 8 ml/L Triton X-100 and 8 g/L WS_2, (f). Transfer film of Au and WS_2 on the worn surface of the ball shown in (c).

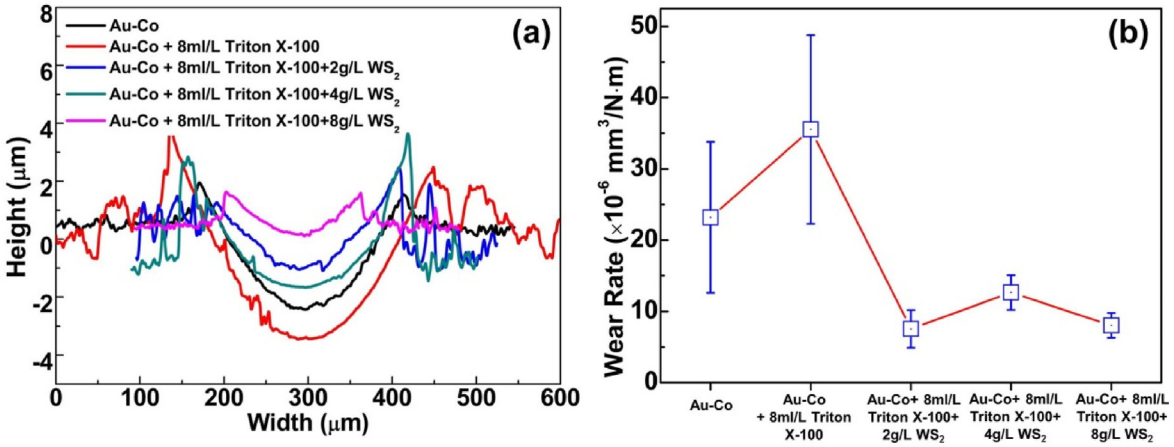

Fig. 15. 2-D profiles of wear tracks (a) and wear rates (b) of different coatings.

Au–Co/WS_2 coating which was obtained from the electrolyte containing 2 g/L WS_2, there were three distinct transition periods observed on the CoF curve, which were induced by the transfer of WS_2 on the ball surface. At last, the CoF stabilized at 0.15. The Au–Co/WS_2 coatings obtained from electrolytes containing 4 g/L and 8 g/L WS_2 showed similar CoF of around 0.05.

As Fig. 14 shows, during the tribological tests, the wear mainly occurred on the Au–Co and Au–Co/WS_2 coatings without noticeable wear happened on the 316L balls. Adding Triton X-100 in the Au–Co electrolyte degraded the wear performance of the Au–Co coating significantly, and the depth of wear track increased from 2 μm to 4 μm (Fig. 15 (a)). This degradation is due to the decrease of Co content in the Au–Co coating, which decreased the coating's hardness accordingly. As Fig. 15 (b) shows, the wear rate of the Au–Co coating (without Triton X-100 in the electrolyte) is 2.3×10^{-5} $mm^3/N \cdot m$. With Triton X-100 added in the electrolyte, the wear rate increased to 3.5×10^{-5} $mm^3/N \cdot m$. When WS_2 is compounded into the Au–Co coating, WS_2-rich Au–Co film transferred from the coating to the ball surface due to adhesive wear (Fig. 14 (f)). The WS_2 films generated both on the coating and ball worn surfaces lubricated the sliding by shearing the weak interlayer bonding in WS_2, which suppressed the adhesion between the two contacting surfaces. With WS_2 lubricating, the wear depths and wear rate were minimized efficiently. The Au–Co/WS_2 composite coating deposited from the electrolyte containing 8 g/L WS_2 has a wear rate of 8×10^{-6} $mm^3/N \cdot m$, which is only 1/3 of the Au–Co coating's wear rate.

4. Conclusion

Au–Co/WS_2 composite coatings with excellent tribological performance were achieved by electrodeposition based on Au–Co acidic cyanide electrolyte. In order to improve WS_2 particles dispersion in the electrolyte probe sonication was applied, which exfoliated and decreased the tungsten disulfide particles size from 2.8 μm to 1.47 μm. Triton X-100 was selected as the surfactant for the dispersion of the WS_2 particles, and its effect on improving the stability of electrolytes which contain WS_2 particles was proved. However, keeping the electrolyte that contains WS_2 particles at 45 °C which is the optimum working temperature of the Au–Co electrolyte, the electrolytes containing 8 ml/L Triton X-100 exhibited phase separation after around 40 min, and such phase separation is caused by the reaching of cloud point of Triton X-100 in the Au–Co base electrolyte. With the assist of Triton X-100, Au–Co/

WS_2 composite coatings were deposited under a current density of 5 A/dm^2. The adding of Triton X-100 and WS_2 in the Au−Co electrolyte has a noticeable effect on the deposition rate and Co content in the composite coating. With WS_2 concentration increase, the surface roughness and crystallite size of the Au−Co/WS_2 composite coatings increased accordingly. The Au−Co/WS_2 composite coatings developed showed excellent tribological performance. With WS_2 presence in the coating, the lowest CoF and wear rate achieved are 0.05 and 8×10^{-6} mm^3/N·m, respectively.

Declaration of competing interest

The authors of this manuscript certify that they have NO affiliations with or involvement in any organization or entity with any financial interest (such as honoraria; educational grants; participation in speakers' bureaus; membership, employment, consultancies, stock ownership, or other equity interest; and expert testimony or patent-licensing arrangements), or non-financial interest (such as personal or professional relationships, affiliations, knowledge or beliefs) in the subject matter or materials discussed in this manuscript.

CRediT authorship contribution statement

Zhaoxi Chen: Writing - original draft, Writing - review & editing, Conceptualization, Funding acquisition, Formal analysis, Data curation. **Julien Wagner:** Writing - original draft, Writing - review & editing. **Viviane Turq:** Writing - original draft, Writing - review & editing. **Julien Hillairet:** Writing - original draft, Writing - review & editing. **Pierre-Louis Taberna:** Writing - original draft, Writing - review & editing. **Raphael Laloo:** Writing - original draft, Writing - review & editing. **Sandrine Duluard:** Writing - original draft, Writing - review & editing. **Jean-Michel Bernard:** Writing - original draft, Writing - review & editing. **Yuntao Song:** Writing - original draft, Writing - review & editing. **Qingxi Yang:** Writing - original draft, Writing - review & editing. **Kun Lu:** Writing - original draft, Writing - review & editing. **Yong Cheng:** Writing - original draft, Writing - review & editing.

Acknowledgment

The authors would like to show thanks to Stéphane Le Blond Du Plouy from the Centre of Castaing (Espace Clément Ader) for providing the SEM images.

References

[1] Y. Wang, Y. Ju, S. Wei, W. Lu, B. Yan, W. Gao, Mechanical properties and microstructure of Au−Ni−TiO 2 nano-composite coatings, Mater. Char. 102 (2015) 189−194.
[2] M. Hosseini, S. Ebrahimi, The effect of Tl (I) on the hard gold alloy electrodeposition of Au−Co from acid baths, J. Electroanal. Chem. 645 (2010) 109−114.
[3] Z. Chen, J. Hillairet, V. Turq, Y. Song, R. Laloo, J. Bernard, et al., Characterizations of thermal stability and electrical performance of Au-Ni coating on CuCrZr substrate for high vacuum radio-frequency contact application, Thin Solid Films 659 (2018) 81−88.
[4] S. Dimitrijević, M. Rajčić-Vujasinović, V. Trujić, Non-cyanide electrolytes for gold plating−a review, Int. J. Electrochem. Sci 8 (2013) 6620−6646.
[5] N. Togasaki, Y. Okinaka, T. Homma, T. Osaka, Preparation and characterization of electroplated amorphous gold−nickel alloy film for electrical contact applications, Electrochim. Acta 51 (2005) 882−887.
[6] N. Yamachika, Y. Musha, J. Sasano, K. Senda, M. Kato, Y. Okinaka, et al., Electrodeposition of amorphous Au−Ni alloy film, Electrochim. Acta 53 (2008) 4520−4527.
[7] D. Liang, G. Zangari, Underpotential codeposition of Au-Ni alloys: the influence of applied potential on phase separation and microstructure, J. Electrochem. Soc. 163 (2016) D3020−D3026.
[8] T. Yokoshima, A. Takanaka, T. Hachisu, A. Sugiyama, Y. Okinaka, T. Osaka, Mechanical and electrical properties of Au-Ni-C alloy films produced by pulsed current electrodeposition, J. Electrochem. Soc. 160 (2013) D513−D518.
[9] L. Chalumeau, M. Wery, H. Ayedi, M. Chabouni, C. Leclere, Development of a new electroplating solution for electrodeposition of Au−Co alloys, Surf. Coating. Technol. 201 (2006) 1363−1372.
[10] G. Holmbom, B. Jacobson, J. Sundgren, Composition, structure & hardness of pulse-plated nickel-hardened gold films, in: Proc. Of the AESF Annual Technical Conference. Baltimore, 1995.
[11] P. Narasimman, M. Pushpavanama, V. Periasamyb, Effect of surfactants on the electrodeposition of Ni-SiC composites, Port. Electrochim. Acta 30 (2012) 1−14.
[12] F. Walsh, C. Ponce de Leon, A review of the electrodeposition of metal matrix composite coatings by inclusion of particles in a metal layer: an established and diversifying technology, Transactions of the IMF 92 (2014) 83−98.
[13] M. Alishahi, S.M. Monirvaghefi, A. Saatchi, S.M. Hosseini, The effect of carbon nanotubes on the corrosion and tribological behavior of electroless Ni−P−CNT composite coating, Appl. Surf. Sci. 258 (2012) 2439−2446.
[14] J. Chen, J. Li, D. Xiong, Y. He, Y. Ji, Y. Qin, Preparation and tribological behavior of Ni-graphene composite coating under room temperature, Appl. Surf. Sci. 361 (2016) 49−56.
[15] Y. Jeon, J. Byun, T. Oh, Electrodeposition and mechanical properties of Ni−carbon nanotube nanocomposite coatings, J. Phys. Chem. Solid. 69 (2008) 1391−1394.
[16] Z. Ren, N. Meng, K. Shehzad, Y. Xu, S. Qu, B. Yu, et al., Mechanical properties of nickel-graphene composites synthesized by electrochemical deposition, Nanotechnology 26 (2015), 065706.
[17] G. Yasin, M.A. Khan, M. Arif, M. Shakeel, T.M. Hassan, W.Q. Khan, et al., Synthesis of spheres-like Ni/graphene nanocomposite as an efficient anti-corrosive coating; effect of graphene content on its morphology and mechanical properties, J. Alloys Compd. 755 (2018) 79−88.
[18] C. Liu, F. Su, J. Liang, Producing cobalt−graphene composite coating by pulse electrodeposition with excellent wear and corrosion resistance, Appl. Surf. Sci. 351 (2015) 889−896.
[19] A.K. Behera, A. Mallik, Ultrasound assisted electroplating of nano-composite thin film of Cu matrix with electrochemically in-house synthesized few layer graphene nano-sheets as reinforcement, J. Alloys Compd. 750 (2018) 587−598.
[20] K. Wong, X. Lu, J. Cotter, D. Eadie, P. Wong, K. Mitchell, Surface and friction characterization of MoS2 and WS2 third body thin films under simulated wheel/rail rolling−sliding contact, Wear 264 (2008) 526−534.
[21] Y. He, W. Sun, S. Wang, P. Reed, F. Walsh, An Electrodeposited Ni-P-WS 2 Coating with Combined Super-hydrophobicity and Self-Lubricating Properties, Electrochimica Acta, 2017.
[22] J. Zhou, G. Zhao, J. Li, J. Chen, S. Zhang, J. Wang, et al., Electroplating of non-fluorinated superhydrophobic Ni/WC/WS2 composite coatings with high abrasive resistance, Appl. Surf. Sci. 487 (2019) 1329−1340.
[23] Y. He, S. Wang, W. Sun, P.A. Reed, F.C. Walsh, Synthesis and properties of electrodeposited Ni−Co/WS2 nanocomposite coatings, Coatings 9 (2019) 148.
[24] F. Kopnov, A. Yoffe, G. Leitus, R. Tenne, Transport properties of fullerene-like WS_2 nanoparticles, Phys. Status Solidi 243 (2006) 1229−1240.
[25] N. Zhou, S. Wang, F.C. Walsh, Effective particle dispersion via high-shear mixing of the electrolyte for electroplating a nickel-molybdenum disulphide composite, Electrochim. Acta 283 (2018) 568−577.
[26] M. Rezrazi, M. Doche, P. Bercot, J. Hihn, Au−PTFE composite coatings elaborated under ultrasonic stirring, Surf. Coating. Technol. 192 (2005) 124−130.
[27] R. Mardani, A. Asrar, H. Ershadifar, The effect of surfactant on the structure, composition and magnetic properties of electrodeposited CoNiFe/Cu microwire, Mater. Chem. Phys. 211 (2018) 160−167.
[28] R. Stavitsky, Electroless Gold Plating Solutions, US Patent, Kanto Chemical Co Inc, 1990.
[29] Z. Chen, J. Hillairet, V. Turq, Y. Song, Q. Yang, G. Lombard, et al., Multifunctional tribometer development and performance study of CuCrZr-316L material pair for ITER application, Tribol. Int. 116 (2017) 208−216.
[30] X. Qi, Y.n. Dong, H. Wang, C. Wang, F. Li, Application of Turbiscan in the homoaggregation and heteroaggregation of copper nanoparticles, Colloid. Surface. Physicochem. Eng. Aspect. 535 (2017) 96−104.
[31] C. Delgado-Sánchez, V. Fierro, S. Li, A. Pasc, A. Pizzi, A. Celzard, Stability analysis of tannin-based foams using multiple light-scattering measurements, Eur. Polym. J. 87 (2017) 318−330.
[32] Y. Ren, J. Zheng, Z. Xu, Y. Zhang, J. Zheng, Application of Turbiscan LAB to study the influence of lignite on the static stability of PCLWS, Fuel 214 (2018) 446−456.
[33] F. Gastone, T. Tosco, R. Sethi, Green stabilization of microscale iron particles using guar gum: bulk rheology, sedimentation rate and enzymatic degradation, J. Colloid Interface Sci. 421 (2014) 33−43.
[34] S. Sharma, S. Bhagat, J. Singh, R.C. Singh, S. Sharma, Luminescence in 2-dimensional WS2 nanosheets, in: AIP Conference Proceedings, AIP Publishing, 2018, 030131.
[35] M. Krause, M. Viršek, M. Remškar, N. Salacan, N. Fleischer, L. Chen, et al., Diameter and morphology dependent Raman signatures of WS2 nanostructures, ChemPhysChem 10 (2009) 2221−2225.
[36] V. Štengl, J. Tolasz, D. Popelková, Ultrasonic preparation of tungsten disulfide single-layers and quantum dots, RSC Adv. 5 (2015) 89612−89620.
[37] A. Berkdemir, H.R. Gutiérrez, A.R. Botello-Méndez, N. Perea-López, A.L. Elías, C.-I. Chia, et al., Identification of individual and few layers of WS 2 using Raman Spectroscopy, Sci. Rep. 3 (2013) 1755.

[38] Y.-Y. Yeh, W.-H. Chiang, W.-R. Liu, Synthesis of few-layer WS2 by jet cavitation as anode material for lithium ion batteries, J. Alloys Compd. 775 (2019) 1251–1258.
[39] Q.-A. Poutrel, Z. Wang, D. Wang, C. Soutis, M. Gresil, Effect of pre and post-dispersion on electro-thermo-mechanical properties of a graphene enhanced epoxy, Appl. Compos. Mater. 24 (2017) 313–336.
[40] H. Wang, Dispersing carbon nanotubes using surfactants, Curr. Opin. Colloid Interface Sci. 14 (2009) 364–371.
[41] R. Rastogi, R. Kaushal, S. Tripathi, A.L. Sharma, I. Kaur, L.M. Bharadwaj, Comparative study of carbon nanotube dispersion using surfactants, J. Colloid Interface Sci. 328 (2008) 421–428.
[42] Y. Geng, M.Y. Liu, J. Li, X.M. Shi, J.K. Kim, Effects of surfactant treatment on mechanical and electrical properties of CNT/epoxy nanocomposites, Compos. Appl. Sci. Manuf. 39 (2008) 1876–1883.
[43] B. Valaulikar, C. Manohar, The mechanism of clouding in triton X-100: the effect of additives, J. Colloid Interface Sci. 108 (1985) 403–406.
[44] Z. Wang, J.-H. Xu, W. Zhang, B. Zhuang, H. Qi, Cloud point of nonionic surfactant Triton X-45 in aqueous solution, Colloids Surf. B Biointerfaces 61 (2008) 118–122.
[45] K. Nayana, T. Venkatesha, Synergistic effects of additives on morphology, texture and discharge mechanism of zinc during electrodeposition, J. Electroanal. Chem. 663 (2011) 98–107.
[46] A. Gomes, M. da Silva Pereira, Pulsed electrodeposition of Zn in the presence of surfactants, Electrochim. Acta 51 (2006) 1342–1350.
[47] N. Loukil, M. Feki, Synergistic effect of triton X100 and 3-hydroxybenzaldehyde on Zn-Mn electrodeposition from acidic chloride bath, J. Alloys Compd. 719 (2017) 420–428.
[48] J. Schroers, B. Lohwongwatana, W.L. Johnson, A. Peker, Precious bulk metallic glasses for jewelry applications, Mater. Sci. Eng., A 449 (2007) 235–238.
[49] Y.-A. Kim, Eects of surfactant addition on crystal orientation in alkaline-free electroless copper plating, J. Kor. Phys. Soc. 33 S138S141.
[50] S. Jo, D. Costanzo, H. Berger, A.F. Morpurgo, Electrostatically induced superconductivity at the surface of WS_2, Nano Lett. 15 (2015) 1197–1202.
[51] S.P. Vattikuti, C. Byon, V. Chitturi, Selective hydrothermally synthesis of hexagonal WS_2 platelets and their photocatalytic performance under visible light irradiation, Superlattice. Microst. 94 (2016) 39–50.
[52] A. Monshi, M.R. Foroughi, M.R. Monshi, Modified Scherrer equation to estimate more accurately nano-crystallite size using XRD, World J. Nano Sci. Eng. 2 (2012) 154–160.
[53] E. García-Lecina, I. García-Urrutia, J. Díez, J. Fornell, E. Pellicer, J. Sort, Codeposition of inorganic fullerene-like WS_2 nanoparticles in an electrodeposited nickel matrix under the influence of ultrasonic agitation, Electrochim. Acta 114 (2013) 859–867.